IR and UV Spectroscopy of Vapor-Phase Jet-Cooled Ionic Liquid [emim](+)[Tf2N](-): Ion Pair Structure and Photodissociation Dynamics

ARTICLE *in* THE JOURNAL OF PHYSICAL CHEMISTRY A · OCTOBER 2013

Impact Factor: 2.69 · DOI: 10.1021/jp409670n · Source: PubMed

5 AUTHORS, INCLUDING:

Alexander M. Zolot
Stable Laser Systems, LLC
28 PUBLICATIONS **225** CITATIONS
SEE PROFILE

Jerry Boatz
United States Air Force
199 PUBLICATIONS **13,928** CITATIONS
SEE PROFILE

THE JOURNAL OF PHYSICAL CHEMISTRY A

Article

pubs.acs.org/JPCA

IR and UV Spectroscopy of Vapor-Phase Jet-Cooled Ionic Liquid $[emim]^+[Tf_2N]^-$: Ion Pair Structure and Photodissociation Dynamics

Russell Cooper,[†] Alexander M. Zolot,[†,‡,∥] Jerry A. Boatz,[§] David P. Sporleder,[†,⊥] and Jaime A. Stearns*[,†]

[†]Space Vehicles Directorate, Air Force Research Laboratory, Kirtland AFB, New Mexico 87117, United States

[‡]Institute for Scientific Research, Boston College, Chestnut Hill, Massachusetts 02467, United States

[§]Aerospace Systems Directorate, Air Force Research Laboratory, Edwards AFB, California 93524, United States

Supporting Information

ABSTRACT: Small gas-phase clusters (ion pairs) of the ionic liquid $[emim]^+[Tf_2N]^-$ have been generated in a supersonic expansion. Clusters are investigated via UV photofragmentation and time-of-flight mass spectrometry. Spectra between 42 000 and 45 000 cm^{-1} reveal dynamical branching between direct dissociation of the ion pair to the cation and anion and to radical species. The IR spectrum between 2800 and 3200 cm^{-1} was measured by action spectroscopy. Multiple conformations of the ion pair are found to be present in the molecular beam, leading to broad spectral features, further complicated by hydrogen bonding and Fermi resonances. The measured and theoretical spectra compare well, and the jet-cooled ion pair structures present in the molecular beam are strongly hydrogen bonded "stacked" conformers.

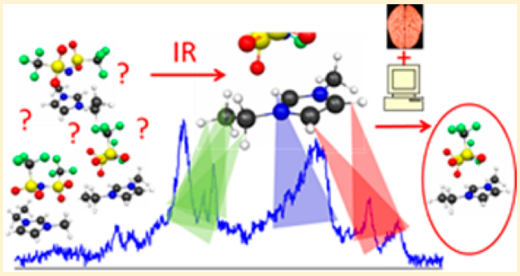

INTRODUCTION

Ionic liquids (ILs) have generated a great deal of attention from the chemical industry and fundamental chemistry community over the past decade. Defined as salts with melting points below 100 °C, ILs have unique properties, such as low vapor pressure, high thermal stability, and good conductivity, motivating a wide array of applications. Proposed uses for ILs include replacements for volatile organic solvents for industrial processes, solvents for carbon dioxide scrubbing, matrices for mass spectrometry, battery electrolytes, and many more.[1] The aerospace community is also interested in ILs as propellants for ion propulsion[2,3] and as a safer replacement for hydrazine in hypergolic fuels.[4−8]

ILs typically consist of organic cations paired with organic or inorganic anions, although the anions can be monatomic.[9] Each IL component can be modified with various functional groups or atomic substitutions, giving rise to a large number of pairwise IL combinations, with tertiary or higher mixtures expanding even further the number of potential ILs for a given application. These simple chemical modifications and mixtures drastically alter the bulk IL properties, including melting point, viscosity, reactivity, solvation, miscibility with other compounds, and so on. Thus, ILs are often touted as customizable.[1] It is exactly this customizability, however, that makes finding the ideal IL for a given application such a daunting task. Synthesizing and experimentally characterizing all possible ILs is an unrealistic proposition. Theoretical treatment provides a more efficient avenue to characterize potential ILs, but methods such as density functional theory, ideal for high throughput, may not be suitable for the weak interion interactions (e.g., van der Waals, hydrogen bonding, π stacking...) found in ILs. More reliable (but expensive) methods such as MP2 still require experimental validation. Thus, the vast modification space of ILs has only begun to be explored, and the need for a predictive understanding of the physical properties of new ionic liquids drives much of the fundamental physical chemistry research on them.

Several theoretical studies have investigated IL *ion pairs*, i.e., small gas-phase clusters made up of one anion and one cation.[10−14] In the absence of detailed experimental measurements of ion pairs, these studies have generally sought to explain bulk properties such as viscosity and melting point. However, extrapolating from the structure of ion pairs to macroscopic properties is tenuous, and detailed experimental investigations of basic properties, such as the physical structure of ion pairs, would provide valuable benchmarks for these fundamental calculations. Unfortunately, FTIR studies of the bulk liquid,[13,15−20] small clusters in cryogenic matrices,[21−23] and vapor at high temperature[19,24] reveal only broad spectral features that are difficult to interpret using theoretical predictions of isolated gas-phase clusters. Studies of IL vapor are a relatively new development, following the demonstration in 2006 that ILs have a finite, if small, vapor pressure at elevated temperatures.[25] The resulting flurry of experimental studies of ILs in the gas phase include verification that, for aprotic ionic liquids, the vapor consists of ion pairs.[24,26−33] Gas-phase VUV dissociation and dissociative photoionization studies have provided valuable insight into the fragmentation of the ion pairs following UV excitation, but such high-energy excitation results in featureless spectra and little insight into the detailed

Received: September 27, 2013
Revised: October 31, 2013
Published: October 31, 2013

structure of the vapor.[29,30] Very recent IR spectroscopy of ionic liquids in helium nanodroplets provided the first experimental comparison for calculations of an ion pair.[33] The present study utilizes IR spectral measurements of cold gas-phase ion pairs and compares them directly to theoretical calculations of the ion pair. Our benchmark measurements are a key step in validating theoretical approaches, providing a solid foundation for calculations extrapolating to IL properties of the bulk, in cryogenic matrices, or in the gas phase at high temperature.

We chose the IL 1-ethyl-3-methylimidazolium bis-(trifluoromethylsulfonyl)imide, abbreviated $[emim]^+[Tf_2N]^-$, shown in Scheme 1, for this preliminary study. This IL is a benchmark system and has been the focus of multiple gas and solution-phase studies and is of particular relevance in electric satellite propulsion as the only space-qualified IL.[2,15,16,21,23,27,28,33−36] Furthermore, $[emim]^+[Tf_2N]^-$ has a relatively high vapor pressure and high decomposition temperature compared to other ILs, making it experimentally convenient for gas-phase studies utilizing thermal vaporization.[37]

Scheme 1. Structure of $[emim]^+[Tf_2N]^-$ Ion Pair with the Imidazole Ring Carbon Positions Labeled

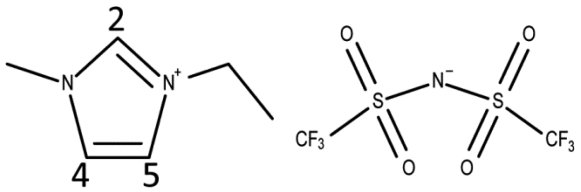

A broad range of experimental and theoretical investigations utilizing IR spectroscopy of bulk $[emim]^+[Tf_2N]^-$ has not yet reached a consensus on the structure of this common IL, or even found agreement on the nature of the binding between the ionic components. Various computational studies have predicted conflicting $[emim]^+[Tf_2N]^-$ ion pair structures, typically falling into two types: "in-plane", in which the anion is predominantly in the plane of the $[emim]^+$ ring, and "stacked," in which the anion sits on top of the cation.[21,23,24,27,33,35,36] Fortunately, a strong indicator of such structural differences is found in the stretching vibration of the $[emim]^+$ C2 and its lone H, Scheme 1. Specifically, as the most acidic bond in $[emim]^+$, C2−H often strongly interacts with the neighboring anion, such that the C2−H stretching frequency shifts and changes intensity as the ion pair structure changes. Evidence for the important role of these interactions in the IL structure comes from Noack et al., who showed that methylation of C2 leads to dramatic changes in the physical properties of the IL, such as viscosity.[13] In the bulk liquid $[emim]^+[Tf_2N]^-$ the C2−H stretch is red-shifted by about 50 cm^{-1}; however, spectral congestion makes the relative roles of hydrogen bonding, coupling with overtones of the in-plane ring modes, and multiple conformations debatable.[15,16,18,35,38,39] Deuteration of the C2−H did not settle this debate, and the exact nature of the interaction between the cation and anion in the bulk remains uncertain.[16] In a neon matrix the structure of the $[emim]^+[Tf_2N]^-$ ion pair is tentatively assigned to "in-plane" and, although the bulk liquid structure could not be determined, there were clues that it differed from the ion pair in the matrix.[23] Such neon matrix studies found that B3LYP is not acceptable for calculating the ion pair structure, for both $[emim]^+[Tf_2N]^-$ and other ionic liquids.[21−23] The extent to which any of these conclusions apply to small IL clusters in the gas phase is unknown, but recent studies of the ion pair in helium droplets show stacked structures to be present in the gas phase.[33]

This study attempts to settle this uncertainty, presenting for the first time the IR (2800−3200 cm^{-1}) and UV (42 000−45 000 cm^{-1}) spectroscopy of jet-cooled $[emim]^+[Tf_2N]^-$ ion pairs. UV spectroscopy reveals two different photofragmentation pathways, providing insight into the photodissociation dynamics of the ion pair. IR/UV double resonance provides the high sensitivity needed to probe the IR absorption of $[emim]^+[Tf_2N]^-$ ion pairs at molecular beam densities. The jet-cooled IR technique simplifies the spectrum and produces narrower features compared to high-temperature and condensed-phase studies. High-level ab initio calculations of ion pair geometries and harmonic vibrational frequencies confirm the C2−H stretch to be a highly sensitive marker of structure. Measurements and calculations agree that the "stacked" conformations of the $[emim]^+[Tf_2N]^-$ ion pair are energetically favored over "in-plane". We group the "stacked" predictions into three families and find that ion pairs in the molecular beam belong to the strongly hydrogen-bonded family. The broad, temperature-dependent spectral feature in the C2−H stretch region indicates rich cation/anion interactions, in which hydrogen bonding, Fermi resonances, and the presence of multiple conformations are all likely to play a role. These results serve as a benchmark for computational studies as well as a base for understanding the IR spectra of imidazolium-based ionic liquids in the liquid phase.

EXPERIMENTAL METHODS

The experimental apparatus for IR/UV double resonance spectroscopy resembles those reported previously.[40] A rough outline of the apparatus is presented here, with emphasis upon the most unique feature, a supersonic jet expansion containing $[emim]^+[Tf_2N]^-$ vapor that enables the vapor to be studied by use of established molecular beam techniques. The development of jet-entrained IL vapor builds upon extensive recent work on the production and nature of ILs in the gas phase. Indeed, ILs generally have extremely low vapor pressures at room temperature, and chemical decomposition upon heating is a major concern.

We produce IL vapor by placing a small glass vial with ∼0.1 mL IL within a stainless steel gas line, maintained at ∼230 °C. This vapor diffusively mixes with helium carrier gas and enters the vacuum through a general valve heated to ∼215 °C. At 230 °C $[emim]^+[Tf_2N]^-$ has a vapor pressure of approximately 1.0×10^{-3} Torr, as measured by thermogravimetric analysis.[36] In practice, the sample lasts for weeks before decomposition of the sample and/or valve materials interferes with IL vapor delivery, at which point the valve is serviced and sample replaced. Thermal engineering of the delivery system must avoid (i) overheating the sample or portion of the gas line, which may cause excessive decomposition of the IL, (ii) damaging the pulsed valve by overheating, and (iii) generating cold spots where the gaseous sample will condense. When these conditions are avoided, a jet containing trace vapor of IL ion pairs is generated and can be utilized in various molecular beam experiments, such as the IR/UV double resonance time-of-flight (TOF) mass spectrometer used in this work.

The supersonic jet of $[emim]^+[Tf_2N]^-$ in helium carrier gas (P = 1650 Torr) originates from the pulsed valve orifice (200 μm, Δt ∼500 μs) at 10 Hz, and the expanding gas cools the

dx.doi.org/10.1021/jp409670n | J. Phys. Chem. A 2013, 117, 12419−12428

internal degrees of freedom of the ion pair. The exact internal state distribution of the ion pairs is not known; however, supersonic expansions of similarly sized polyatomic molecules generally remove vibrational hot bands and have rotational temperature of less than 20 K.[40] The extent of conformational cooling is complicated and depends on the barriers between the conformations as well as the rate of cooling.[41,42] The beam is skimmed, and tunable UV light from a frequency doubled 10 Hz dye laser passes through an $f = \sim 50$ cm lens, intersecting the molecular beam 19 cm downstream from the valve orifice. This UV pulse produces charged fragments, which are detected with an RM Jordan TOF mass spectrometer perpendicular to the plane of the laser and molecular beams. We are able to detect both cations and anions, although not simultaneously.

The IR spectrum is measured by use of a LaserVision tunable Nd:YAG-pumped optical parametric converter with separate oscillation and amplification stages, which produces 18 mJ pulses in the C−H stretch region between 2800 and 3200 cm^{-1}.[16,34] The IR and UV lasers counterpropagate through the TOF source region and the $[emim]^+$ signal is recorded while tuning the IR laser frequency at 0.3 cm^{-1}/point. The IR laser pulses at 5 Hz, and the UV laser pulses at 10 Hz. The resulting signal is averaged for 10 s on two separate channels, UV only and IR+UV, generating the IR response and background curves simultaneously. When acquiring IR spectra, the UV laser is maintained at 230 nm, a wavelength longer than that producing strong UV signal, as discussed in more detail in the following section. The experimental timing is such that the IR laser passes through the molecular beam 20 ns before the UV. Absorption of an IR photon increases the probability for UV dissociation of the ion pair, and consequently a gain in ion signal when the IR laser is resonant with an absorption in the ion pair.

RESULTS AND DISCUSSION

Mass Spectrometry. Representative mass spectra acquired at a UV wavelength of 222.5 nm are presented in Figure 1. The

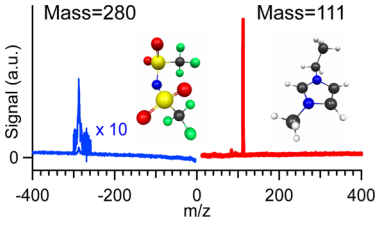

Figure 1. Mass spectra following fragmentation of $[emim]^+[Tf_2N]^-$ by 222.5 nm light. The blue corresponds to negatively charged particles and the red to positively charged particles. The peak in the anion mass spectra arises from the intact $[Tf_2N]^-$ at mass 280 and the largest cation peak is at mass 111, corresponding to the intact $[emim]^+$.

present mass spectra contain both the cation and anion moieties, and are consistent with previous studies showing that the primary mechanism for evaporation of $[emim]^+[Tf_2N]^-$ is via ion pairs,[24,27,28,32] though the present TOF apparatus would not be sensitive to bare ions or charged clusters originating from the pulsed valve.

As seen in Figure 1, the mass spectra are quite clean, with an absence of fragmentation of the ions following UV absorption and minimal decomposition products from the thermal vaporization source. The detection efficiency of the anion and cation has not been quantified, but they are likely to be similar. Consequently, we attribute the much smaller anion signal (about 1/100th of that obtained with the cation) to the presence of multiple dissociation mechanisms, to be discussed in the following section.

UV Spectroscopy. We record the UV spectrum by integrating a single peak of the mass spectrum, either the intact cation or anion, as a function of the UV wavelength. Figure 2a presents the results of such measurements, averaging

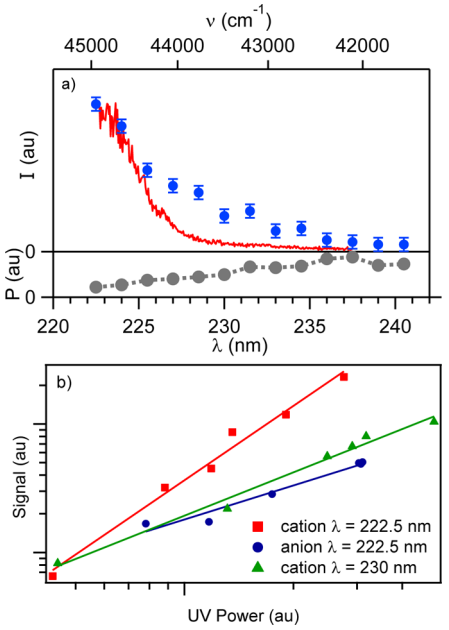

Figure 2. (a) Wavelength-dependent signal for generating anion, blue circles, and cation, red line. Intensities have been corrected linearly by the measured laser power, also provided as the gray line and points. The anion signal was acquired at approximately 4 times higher gain and has been multiplied by 35 to be on the same scale as the cation signal. The anion error bars represent one standard deviation. (b) Measurements of cation and anion signal as a function of UV laser power at the UV wavelength indicated. Linear least-squares fits through log−log plots produce power dependent exponents of 1.92 ± 0.13, 0.88 ± 0.09, and 1.12 ± 0.07 for the cation 222.5 nm, anion 222.5 nm, and cation 230 nm data, respectively.

50 shots per point for the cation and 5000 shots for the anion to compensate for the lower signal level apparent in Figure 1. For ease of presentation, the spectra are linearly scaled by laser power, also shown in Figure 2a, and although this scaling is not correct for the cation at shorter wavelengths it does not change the interpretation of the data. The error bars on the anion data points are the standard deviation of five measurements of the mass spectrum's baseline, generated by use of the same integration algorithm that produces the signal. Additional measurements show that strong ion signal production extends to the blue at least as far as 210 nm, the physical limit of our UV generation source. At wavelengths longer than 223 nm, the creation of $[emim]^+$ decreases and is near zero by 235 nm. The anion UV dependence follows a trend qualitatively similar to that of the cation.

Previous UV absorbance measurements of hot gas-phase $[emim]^+[Tf_2N]^-$ and related ILs have reported similarly broad UV spectra, though the underlying physics was not discussed.[31,43] At such elevated temperatures the onset to absorption occurs slightly to the red of that seen in Figure 2a, likely due to higher-energy conformations as well as internally excited rotational and vibrational states making the excited state

dx.doi.org/10.1021/jp409670n | J. Phys. Chem. A 2013, 117, 12419−12428

accessible at lower UV energies in a manner similar to that used in our IR/UV double resonance measurements in the following section. Gas-phase studies of imidazole have also reported broad UV absorption, very similar to the ion pair UV absorbance we report here, attributed to the coupling of the bright electronically excited state to a dark dissociative state.[44,45] We propose a similar explanation for this broadness seen in the UV spectrum of $[emim]^+[Tf_2N]^-$, namely that the bright electronically excited state is coupled with a dark dissociative or very weakly bound excited state.

Subtle differences between the UV spectra in Figure 2a indicate differing photoinduced dynamics for production of the two ion species. Although it is also possible that these different mechanisms could arise from different ion pair structures, clusters larger than the ion pair, or contaminating species, the overall similarities for the two pathways and simplicity of the mass spectra indicate this is not the case. Instead, we propose that the spectral differences arise from multiple mechanisms of ion pair dissociation. Because our technique is an action spectroscopy, i.e., signal intensity reports on the photon absorption probability modified by the efficiency of creating ions, dynamic effects can directly lead to such spectral differences.

The laser power dependence measurements presented in Figure 2b offer insight into the photophysical pathways. At 222.5 nm, the cation signal depends quadratically on laser power, indicating a two-photon process. In contrast, the power dependence of both the anion signal at 222.5 nm and cation signal at 230 nm is linear, meaning these signals are due to single photon events. Thus, most of the cation signal comes from fundamentally different photophysics than that producing anion signal. The changing power dependence with wavelength means the scaling of Figure 2a as presented is imperfect and would require direct measurement of the power dependence of the cation at each wavelength. In the absence of such detailed measurements we note that the normalized cation signal at longer wavelengths would be suppressed when compared to the two-photon signal at shorter wavelengths and lower laser power. Such corrections would only further exaggerate the differences between the two curves in Figure 2a, further highlighting the disparate dynamics between anion and cation production. The different production efficiencies of cation and anion signal could arise from photophysics after dissociation, i.e., photodetachment depletion of the bare anion, which we calculate using M06/6-311++G**[46,47] to require 5.6 eV, very close to our experimental photon energy. Even assuming photodetachment is energetically feasible, the strongest cation signals are clearly obtained through a two-photon process near 222.5 nm, pointing toward a dynamical explanation of the laser power dependence at this wavelength. On the basis of these observations and previous observations of ion pairs dissociating to neutrals following excitation at high photon energy,[28] we propose the mechanism in Figure 3 for the creation of $[emim]^+$ and $[Tf_2N]^-$ from $[emim]^+[Tf_2N]^-$. Absorption of a single UV photon excites the $[emim]^+[Tf_2N]^-$ ion pair from the ground electronic state, black, to a bound electronically excited state, blue, from which the molecule quickly undergoes internal conversion to a weakly bound or purely dissociative electronic state, red. We hypothesize this is a charge transfer state asymptotically corresponding to the dissociated imidazolyl ($[emim]^\bullet$) and imidyl ($[Tf_2N]^\bullet$) radicals. Coupling from the initial electronically excited state to this charge transfer channel is expected to be much faster than relaxation to the ground

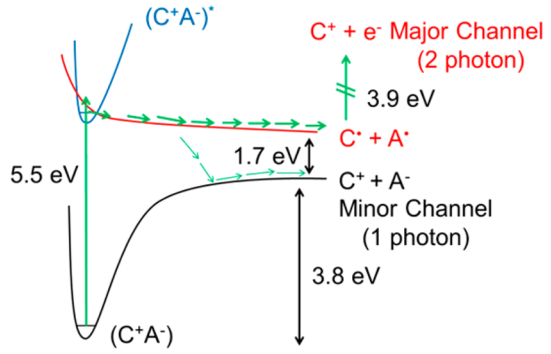

Figure 3. Electronic energy level schematic for $[emim]^+[Tf_2N]^-$. The green arrows represent the possible pathways for ion pair dissociation. The energies shown, except the experimental photon energy of 5.5 eV, are calculated at the M06/6-311++G** level of theory and do not include zero point corrections.

electronic state.[44] Prior to dissociation, a small fraction of charge transfer species do access the ground electronic state or a direct ion-dissociation channel, from which they dissociate into $[emim]^+ + [Tf_2N]^-$, resulting in our weak single-photon anion and cation signal. Ion pairs that remain on the charge transfer surface dissociate to $[emim]^\bullet + [Tf_2N]^\bullet$. These species are not charged and therefore not directly detectable by our technique. However, in our focused UV beam, a second photon readily ionizes $[emim]^\bullet$, forming $[emim]^+ + e^-$. Thus, the strong increase in cation signal at wavelengths shorter than 227 nm is attributed to the onset of charge transfer dynamics followed by subsequent ionization of $[emim]^\bullet$, which only requires 3.9 eV. The neutralized anion, $[Tf_2N]^\bullet$, has a much higher ionization potential of 8 eV and cannot be ionized by a 220 nm photon. The energies in Figure 3 were calculated using M06/6-311++G** on the lowest-energy $[emim]^+[Tf_2N]^-$ conformation found by MP2 (discussed in more detail below) and do not contain zero-point corrections.[46,47] It should be noted that these vary from previously published energies,[28] which we attribute to our use of DFT instead of Hartree−Fock, as well as a different ion pair structure. The two-mechanism scheme in Figure 3 accounts for the differing UV spectra in Figure 2a, the weak anion signal in Figure 1, and the observed power dependences of both the anion and cation signal in various wavelength regimes in Figure 2b.

Although further theoretical work is necessary to firmly establish the states involved in the UV absorption and the mechanism of coupling among the bright excited state, the charge transfer state, and ground electronic state, a number of conclusions can be drawn from these observations about the nature of the excited state dynamics. The relative intensity of the anion and cation signals reveals that the coupling to the ground state is weak. The laser power dependences show that at long wavelength cations are produced almost exclusively by a single photon event, so the cation to anion ratio should be 1. When correcting for detector gain and laser power, we in fact do see that the level of cation and anion signal at wavelengths longer than 231.5 nm is the same within the signal-to-noise. The branching ratio R for the two paths at 222.5 nm has been calculated from the corrected anion A (corresponding to the one-photon signal) and cation C (resulting from both one- and two-photon processes) signal levels via $R = A/(C - A)$. Because not all of the $[emim]^\bullet$ is ionized, we can only arrive at an upper limit of the branching ratio for dissociation to the ion pair. At 222.5 nm the one-photon ion pair dissociation is less

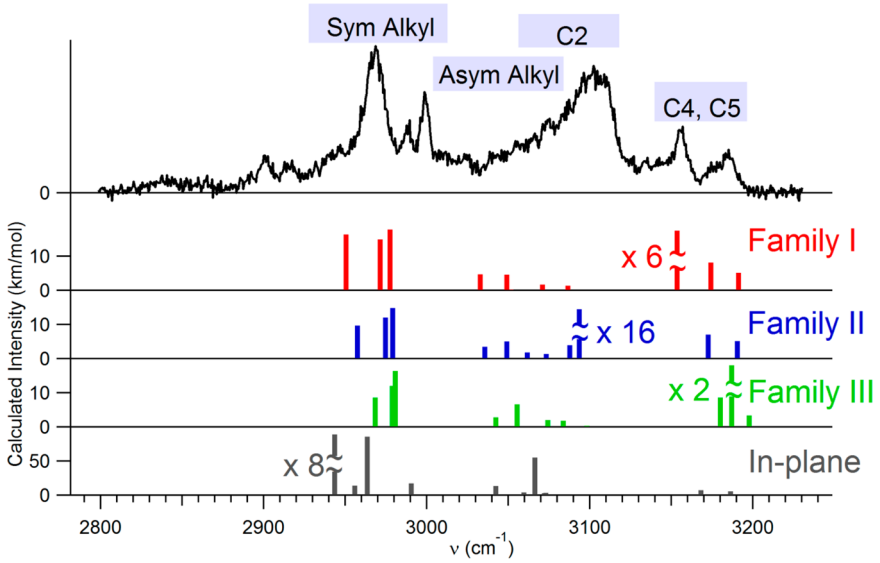

Figure 4. Experimentally measured IR spectrum (top, black) of jet-cooled $[emim]^+[Tf_2N]^-$ vapor, compared to representative theoretically predicted stick spectra, calculated at the MP2/aug-cc-pVTZ level,[48] with frequencies scaled by an empirical factor of 0.96 (lower plots).[49−54] The stick spectrum of the lowest energy isomer for each family type (see text and Table 1) is shown in red, blue, green, and gray, corresponding to family types I, II, III, and in-plane, respectively. All the families exhibit a high-intensity C2−H stretching mode, shown with appropriate multiplication (note the different scale on the bottom trace). The experimental spectrum best matches the calculated spectra of family II.

than 0.7% of the radical dissociation. These dissociation pathways are similar to those reported in recent VUV (17−26 eV) ionization velocity map imaging studies of $[emim]^+[Tf_2N]^-$.[28] However, at those high photon energies direct dissociation dominates, producing $[emim]^+ + [Tf_2N]^-$, with a minor channel producing $[emim]^+ + [Tf_2N]^\bullet + e^-$. Our 5.5 eV data indicate that direct dissociation is also the major channel at wavelengths longer than 230 nm, but the absorption and/or dissociation probability is low. At slightly higher energy, starting around 228 nm, excitation and dissociation increase but the primary dissociation mechanism involves charge transfer and results in radical, not ionic, fragments.

Thus, we conclude that the $[emim]^+[Tf_2N]^-$ ion pairs primarily dissociate via charge transfer to form radical species. The neutralized cation is detected following photoionization by a subsequent photon. The majority of the cation signal comes from this multiphoton process, with less than a percent of the ion pairs undergoing direct dissociation to the cation and the anion at 222.5 nm. The exact nature of the coupling between the charge transfer and ground electronic state is, as of yet, unknown; however, it indicates multiple conical intersections, and a complicated and rich excited electronic state environment. Regardless of the nature of the ionization event, the change in the UV fragment formation due to the absorption of an IR photon enables the IR spectrum of $[emim]^+[Tf_2N]^-$ ion pairs to be investigated with this same experimental apparatus.

IR Spectroscopy. We acquired the IR spectrum of $[emim]^+[Tf_2N]^-$ via UV/IR double resonance action spectroscopy. Figure 4 shows the IR spectrum of $[emim]^+[Tf_2N]^-$ recorded by monitoring the $[emim]^+$ fragment with the UV laser at 230 nm. The IR laser power is relatively constant from 2900 to 3300 cm^{-1} with fluctuations less than 20% and typically much less than 10%. Though the power drops by 25% between 2900 and 2800 cm^{-1}, there are no features in this spectral region.

The IR features of $[emim]^+[Tf_2N]^-$ have been previously assigned for the liquid and gas phases,[24,34] and these previous assignments generally agree with new calculations and the labels provided in Figure 4. All features in this region correspond to C−H stretches of $[emim]^+$. The highest-frequency peaks are the C−H stretches of two ring carbons (C4 and C5), with the peak at 3155 cm^{-1} assigned to the symmetric stretch and the peak at 3185 cm^{-1} to the antisymmetric stretch. The large, broad peak near 3100 cm^{-1} is assigned primarily to the C2−H stretch, although the red tail masks ethyl and methyl asymmetric stretches. The grouping of three peaks between 2950 and 3000 cm^{-1} corresponds to the methyl symmetric stretch (2970 cm^{-1}), the CH_2 symmetric stretch (2990 cm^{-1}), and the ethyl CH_3 symmetric stretch (3000 cm^{-1}). Two small peaks are apparent in our spectrum at 2900 and 2915 cm^{-1} but have no obvious counterpart in the theoretical harmonic spectra or in overtones, and are currently unassigned.

We derive more detail about the nature of the $[emim]^+[Tf2N]^-$ cation−anion interaction by comparing the experimental spectrum to the theoretical spectra of 23 low-energy conformers calculated at the MP2/aug-cc-pVTZ level of theory. Details of the computational methods can be found in ref 33. Table 1 contains a summary of these calculations and shows the energetics, including unscaled zero point vibrational energy corrections, the C2−H stretch frequency and intensity, and "family grouping" by which we have characterized similar spectra from distinct conformers. Only two of these conformers are characterized by the $[Tf_2N]^-$ lying predominantly in the plane of the $[emim]^+$ ring, and they are more than 20 kJ/mol higher in energy than the lowest energy conformer.

The 21 "stacked" conformers in Table 1 have been grouped by their C2−H stretch frequencies into three distinct families, which differ primarily in the orientation of the C2−H of the cation to an oxygen atom on the anion. The two calculated lowest energy structures belong to family I, although the energetics of structures 3−8 are extremely close, at most 7.1 kJ/mol above conformer 1, making them essentially iso-energetic within the accuracy of the calculations. Figure 5 shows the

dx.doi.org/10.1021/jp409670n | J. Phys. Chem. A 2013, 117, 12419−12428

Table 1. Family, Energy, C2−H Stretch Frequency, and Intensity for 23 Low-Energy Conformers

			C2−H stretch	
conformer	family	energy (kJ/mol)	frequency (cm^{-1})	intensity (km/mol)
1	I	0.0	3153	104.6
2	I	1.7	3159	73.9
3	II	3.4	3094	230.7
4	II	4.6	3108	185.6
5	II	6.4	3118	161.4
6	III	7.0	3187	36.0
7	III	7.1	3190	27.5
8	III	7.1	3188	37.0
9	III	9.1	3189	26.5
10	III	11.6	3191	16.0
11	III	12.7	3188	49.2
12	III	13.2	3191	36.9
13	I	14.0	3150	135.1
14	III	14.9	3186	24.4
15	I	16.2	3168	38.4
16	I	16.2	3165	89.9
17	I	16.8	3171	108.1
18	III	17.3	3188	41.3
19	III	18.5	3183	10.9
20	in-plane	21.2	2943	712.8
21	in-plane	24.3	3153	205.0
22	III	38.4	3184	24.7
23	III	43.4	3184	12.7

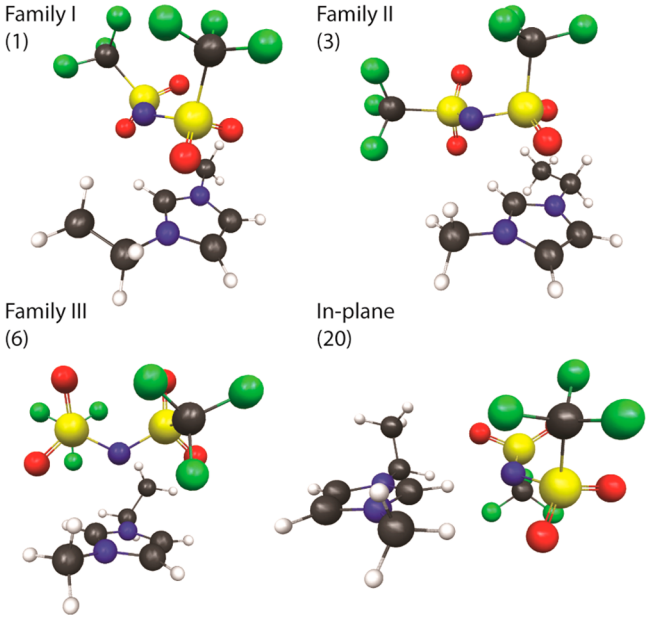

Figure 5. Calculated (MP2/aug-cc-pVTZ[48]) structures of the lowest-energy conformations of each family of $[emim]^+[Tf_2N]^-$. Each structure is designated with the family number followed by the conformation number in parentheses.

calculated geometries for the lowest-energy member of each conformer family. The five lowest-energy conformations, including conformers 1 and 3 shown in Figure 5, show the $[Tf_2N]^-$ nitrogen pointing to one of the alkyl side chains, rather than into the ring or away from the cation, as many of the higher-energy conformers do. Conformations generally also differ in the orientation of the ethyl chain (in or out of the plane of the imidazolium ring), in the anion conformation (cis, trans, etc), and in the relative orientation of the cation and anion (e.g., alignment of the C2−H axis with the S−S axis). These different degrees of freedom combine to give varying levels of interaction between the C2−H and the anion SO_2 groups. As Figure 5 shows, one SO_2 group of the anion interacts with the C2−H in each "stacked" conformation, but the strength of this interaction depends on the other conformational details. Thus, although the C2−H frequency is a convenient metric of the ion pair structure, it alone cannot capture all the structural features of the ion pair nor is it directly related to the ion pair energy.

Figure 4 compares the experimental IR spectrum to the calculated spectra of the lowest-energy member of each of the four families of structures, specifically conformers 1, 3, 6, and 20. Our present results preclude the possibility of the "in-plane" ion pair structures, which would result in a more intense C2−H stretch absorption near 2940 cm^{-1}, and our spectrum more clearly agrees with the class of conformers where $[Tf_2N]^-$ is "stacked" on top of the $[emim]^+$ ring. From this we can conclude that any theoretical method that favors the "in-plane" arrangement does not reproduce experiment. This observation agrees with some previous theoretical results predicting that the less basic, less coordinating anions, such as $[Tf_2N]^-$, prefer the "stacked" structure[10] and contradicts previous reports of "in-plane" lowest energy conformers.[23] The predominant species in the molecular beam are from family II, which exhibits the strongest hydrogen bond of the stacked conformations. The three members of family II, conformers 3−5, possess C2−H frequencies of 3094, 3108, and 3118 cm^{-1}, spanning most of the broadest experimental peak. Other than the location of the C2−H peak, the calculated spectra of the three members of family II are virtually indistinguishable. Conformer 5, for example, differs from conformer 3 only in that the ethyl group points up toward the anion rather than in the plane of the ring. A more detailed structural assignment of the ion pairs present in the molecular beam is thus hindered by the similarity of many low-lying conformations and the broad absorption features obtained in the present experiment.

Perhaps the most interesting spectroscopic region is the C2−H stretch. This peak is substantially broader than the other peaks and is quite red-shifted from its location in the bare $[emim]^+$ cation (3180 cm^{-1}). Such a red shift is readily explained by strong interactions with the anion.[17−20] Thus, the shape and position of the C2−H stretch is sensitive to the $[emim]^+[Tf_2N]^-$ structure, especially hydrogen bonding between the cation and the anion. The present measurements give strong experimental evidence that the C2−H is hydrogen bonded to the neighboring $[Tf_2N]^-$ anion. However, hydrogen bonding is unlikely to be the only significant broadening mechanism in this region, with conformational heterogeneity and Fermi coupling also likely playing a significant role, in agreement with previous work.[33] Each of these effects will be considered in turn below.

The broadness of the C2−H stretch at 3100 cm^{-1} and calculations revealing three nearly isoenergetic conformers indicate that multiple conformations of the ion pair are present in the molecular beam. We made several UV wavelength scans with various fixed IR laser frequencies, in an effort to distinguish separate ion pair conformations. However, the IR-dependent UV spectra from the different strong peaks and at various points on the broad shoulder of the peak at 3100 cm^{-1} were indistinguishable from each other within signal-to-noise.

dx.doi.org/10.1021/jp409670n | J. Phys. Chem. A 2013, 117, 12419−12428

Due to the similarity of the conformers of family II it is not surprising that the UV absorbance is similar if not identical for these conformations, and although these features likely arise from different conformers, the UV spectrum of each conformer is indistinguishable within our SNR.

The presence of multiple conformations is verified by changing the valve backing pressure resulting in warmer ion pairs. The infrared spectrum of $[emim]^+[Tf2N]^-$ is found to be quite robust with respect to temperature, as shown in Figure 6.

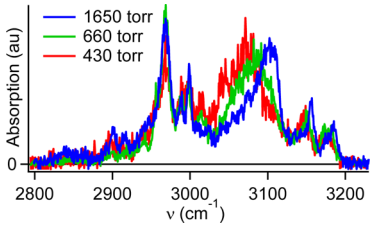

Figure 6. Comparison of infrared spectra acquired under different jet conditions. The blue spectrum was recorded with high (1650 Torr) helium backing pressure and is a repeat of the data presented in the top panel of Figure 4. The green and red spectra were acquired at backing pressures of 660 and 430 Torr, respectively, and thus correspond to progressively warmer jet conditions. Apparent changes in line shapes resulting in more absorption at redder wavelengths are attributed to changing ion pair conformer population in the molecular jet. See text for details.

As expected, the most dramatic change occurs in the C2−H stretch region. Under progressively warmer jet conditions, the peak of the C2−H region shifts from 3100 to 3070 cm^{-1}. For each measured spectrum, significant intensity is observed across a peak in the region from 3030 to 3120 cm^{-1}, but the maximum intensity of the feature shifts to the red as the sample temperature increases. This shift in the peak and therefore the shape of the C2−H region supports the conclusion that multiple conformations are present in the molecular beam and that the width of the peak around 3100 cm^{-1} is caused by a heterogeneous mixture of conformers whose populations shift with jet temperature. In light of the data in Table 1, it is surprising that the peak shifts to the red with increasing temperature, as the higher-energy members of family II as well as all of families I and III show higher-frequency C2−H stretches than does conformer 3. However, because the calculations do not provide the needed accuracy to confidently sort the structures by energy, we cannot say definitively which members of family II exist under which temperatures. It seems clear that the relatively small changes above 3150 cm^{-1} rule out a substantial contribution from families I and III, even under the warmer jet conditions.

In Figure 6, the C4−H and C5−H stretch regions also exhibit red-shifting line profiles, though less dramatically than that observed in the C2−H stretch region. It is likely that different conformations of the anion above the $[emim]^+$ ring directly lead to less dramatic changes to the local environment perturbing these bonds. A small peak is also seen to grow in around 3015 cm^{-1}, and further investigation of this feature is warranted, though it seems likely to be caused by higher energy conformers. Other than the above features, the spectrum shifts very little with temperature.

The recent helium nanodroplet work of Douberly and co-workers,[33] provides a still colder (0.4 K) sample of ion pairs for comparison, though we note that the fast cooling dynamics in droplets likely leads to dynamical trapping of ion pairs in higher energy conformations. Significantly, the present spectrum outside of the 3025−3125 cm^{-1} C2−H stretch region agrees quite well with that measured in helium nanodroplets. In particular, the alkyl stretch regions are remarkably similar. The C2−H region retains some of the strongest lines, but instead of the broad unresolved feature observed here, a series of sharp peaks are resolved. Douberly and co-workers have attributed these features primarily to Fermi coupling between modes in a single species. However, the data in Figure 6 prompt us to assert that the large number of peaks observed in this region could be caused by a distribution of several conformers of family II, which remain populated by the fast cooling dynamics in the nanodroplet medium. By way of support, the nanodroplet results show multiple strong peaks between 3050 and 3075 cm^{-1}, the same region toward which our intensity shifts with increasing temperature. Thus, we assign this region to higher energy family II-type conformations, populated in our jet with increasing temperature, but still present in the nanodroplet experiment, in which rapid cooling can trap population in these higher-energy conformations. Regardless of mechanism, the C2−H stretch region displays significant complexity, resulting in a broadening of this strong line and producing a peak intensity on par with the nearby alkyl stretch transitions.

The droplet study does differ significantly in that Douberly and co-workers have not assigned any spectral features to the C4 and C5−H stretches and have not made any measurements above 3175 cm^{-1}, where we observe the C4 and C5−H antisymmetric stretch. Thus, they assign the peak at 3155 cm^{-1} to the C2−H stretch from family I. Although we cannot rule out the possibility of members of family I producing these features, the calculations indicate that the C4 and C5−H stretches are only a factor of 2 less intense than the alkyl symmetric stretches, so we find it unlikely that the C4 and C5−H stretches are so optically weak as to not be detectable. Additionally, the temperature-dependent measurements in Figure 6 also reveal similar broadening in the lines at 3155 and 3185 cm^{-1}, indicating similar temperature dynamics for these two peaks as might be expected for the tightly coupled C4 and C5−H symmetric and antisymmetric stretches. Neglecting this minor disagreement, the IR spectra reported here and in the nanodroplet study are remarkably similar and much of our analysis reinforces the conclusions from that study.

It is likely that Fermi coupling also contributes to the broad absorption we have observed in the 3100 cm^{-1} region, as previously attributed in this system.[15,33] Previous calculations show large cubic force constants that anharmonically couple the C2−H stretch with the in-plane ring modes overtones and combination bands.[15,16,38] These same studies claim that hydrogen bonding does not play a role in the liquid spectrum; however, Fermi resonances alone could not explain the increased transition intensity, large red shift, and observed temperature sensitivity reported here. Thus the importance of hydrogen bonding cannot be neglected in the isolated ion pair, particularly because a C2−H stretch that has not been red-shifted will have insufficient energetic overlap to significantly couple with the in-plane ring vibration overtones. In contrast, the C4−H and C5−H stretches are not found to be red-shifted, intensified, or significantly coupled to the in-plane ring modes in our current spectrum and theoretical treatments. Other groups have postulated that the close contact between the anion and the C2−H is driven by electrostatics and not

dx.doi.org/10.1021/jp409670n | J. Phys. Chem. A 2013, 117, 12419−12428

hydrogen bonding; however, this interaction perturbs the C2−H stretch in a manner similar to hydrogen bonding, and much of the disagreement simply lies in the definition of the hydrogen bond.[14]

We believe that the width and position of the feature at 3100 cm^{-1} originates from a combination of all the factors discussed above. Hydrogen bonding between the C2−H of the cation and the anion shifts the C2−H stretch to the red and broadens it somewhat. Multiple conformations are present in the beam and each conformation has a different extent of C2−H anion hydrogen bonding, such that multiple broad peaks overlap to give one large, broad spectral feature. The red shift of the C2−H allows for Fermi coupling to in-plane ring modes, perhaps giving rise to even further broadening. Each of these three factors plays a role in the complexity of the C2−H stretch region, and the complicated nature of the interactions is likely the cause of the disagreement in the literature.

CONCLUSIONS

The UV spectrum and photodissociation dynamics and the IR spectrum of cold, isolated ion pairs of $[emim]^+[Tf_2N]^-$ have been characterized for the first time. UV dissociation reveals rich dynamics with most of the ion pairs dissociating to the radical species from a weakly bound or unbound charge transfer state. Fewer than 1% of the ion pairs directly dissociate into the component ions. The observed IR spectrum correlates well with calculations, allowing assignment of its features to specific C−H stretches. The C2−H stretching mode is particularly sensitive to its local environment and is indicative of the ion pair structure. Calculations of the ion pair indicate that the lowest energy structures are "stacked," in agreement with experimental results. Among the many possible "stacked" structures, the family of conformers with the strongest hydrogen bonding is found to most closely match the IR spectrum, with the breadth of the C2−H feature indicating the presence of multiple closely related conformations. Hydrogen bonding plays a critical role for this vibrational mode, broadening it and bringing it into likely Fermi resonance with overtones of the in-plane ring modes. These perturbation factors of the C2−H stretch of the gas-phase ion pairs also likely play a role in the liquid phase leading to the ambiguity of previous interpretations of the IR spectroscopy of the bulk.

ASSOCIATED CONTENT

Supporting Information

XYZ coordinates, unscaled harmonic frequencies, and intensities for the four conformers shown in Figure 4, calculated at the MP2/aug-cc-pVTZ level of theory, and the complete ref 46. This material is available free of charge via the Internet at http://pubs.acs.org.

AUTHOR INFORMATION

Corresponding Author

*J. A. Stearns: e-mail afrl.rvborgmailbox@kirtland.af.mil.

Present Addresses

[‖]A. M. Zolot: Stable Laser Systems, 5733 Central Ave., Boulder, CO 80301.

[⊥]D. P. Sporleder: Applied Materials, 35 Dory Rd., Gloucester, MA 01930.

Notes

The authors declare no competing financial interest.

ACKNOWLEDGMENTS

Funding for this work was provided by the Air Force Office of Scientific Research under the Molecular Dynamics Program. R.C. and D.P.S. acknowledge support from a National Research Council postdoctoral fellowship. We thank Steven Chambreau for many useful discussions. We thank Samuel Collopy, Radley Serafico, and Erwin Beroncal for assisting with work related to this paper. This work was supported in part by a grant of computer time from the Department of Defense (DoD) High Performance Computing Modernization Program, at the Army Research Laboratory, the Air Force Research Laboratory, Engineer Research and Development Center, and Navy DoD Supercomputing Resource Centers (DSRCs).

REFERENCES

(1) Plechkova, N. V.; Seddon, K. R. Applications of Ionic Liquids in the Chemical Industry. *Chem. Soc. Rev.* **2008**, *37*, 123−150.

(2) Chiu, Y. H.; Gaeta, G.; Levandier, D. J.; Dressler, R. A.; Boatz, J. A. Vacuum Electrospray Ionization Study of the Ionic Liquid, [Emim][Im]. *Int. J. Mass Spec.* **2007**, *265*, 146−158.

(3) Donius, B. R.; Rovey, J. L. Ionic Liquid Dual-Mode Spacecraft Propulsion Assessment. *J. Spacecr. Rockets* **2011**, *48*, 110−123.

(4) Schneider, S.; Hawkins, T.; Rosander, M.; Vaghjiani, G.; Chambreau, S.; Drake, G. Ionic Liquids as Hypergolic Fuels. *Energy Fuels* **2008**, *22*, 2871−2872.

(5) Chambreau, S. D.; Schneider, S.; Rosander, M.; Hawkins, T.; Gallegos, C. J.; Pastewait, M. F.; Vaghjiani, G. L. Fourier Transform Infrared Studies in Hypergolic Ignition of Ionic Liquids. *J. Phys. Chem. A* **2008**, *112*, 7816−7824.

(6) Singh, R. P.; Verma, R. D.; Meshri, D. T.; Shreeve, J. M. Energetic Nitrogen-Rich Salts and Ionic Liquids. *Angew. Chem., Int. Ed.* **2006**, *45*, 3584−3601.

(7) Thottempudi, V.; Shreeve, J. M. Synthesis and Promising Properties of a New Family of High-Density Energetic Salts of 5-Nitro-3-trinitromethyl-1H-1,2,4-triazole and 5,5′-Bis(trinitromethyl)-3,3′-azo-1H-1,2,4-triazole. *J. Am. Chem. Soc.* **2011**, *133*, 19982−19992.

(8) Gao, H.; Joo, Y.-H.; Twamley, B.; Zhou, Z.; Shreeve, J. M. Hypergolic Ionic Liquids with the 2,2-Dialkyltriazanium Cation. *Angew. Chem., Int. Ed.* **2009**, *48*, 2792−2795.

(9) Castner, J. E. W.; Wishart, J. F. Spotlight on Ionic Liquids. *J. Chem. Phys.* **2010**, *132*, 120901−9.

(10) Cremer, T.; Kolbeck, C.; Lovelock, K. R. J.; Paape, N.; Wölfel, R.; Schulz, P. S.; Wasserscheid, P.; Weber, H.; Thar, J.; Kirchner, B.; Maier, F.; Steinrück, H.-P. Towards a Molecular Understanding of Cation−Anion Interactions—Probing the Electronic Structure of Imidazolium Ionic Liquids by NMR Spectroscopy, X-Ray Photoelectron Spectroscopy and Theoretical Calculations. *Chem.—Eur. J.* **2010**, *16*, 9018−9033.

(11) Katsyuba, S. A.; Zvereva, E. E.; Vidiš, A.; Dyson, P. J. Application of Density Functional Theory and Vibrational Spectroscopy toward the Rational Design of Ionic Liquids. *J. Phys. Chem. A* **2006**, *111*, 352−370.

(12) Ueno, K.; Tokuda, H.; Watanabe, M. Ionicity in Ionic Liquids: Correlation with Ionic Structure and Physicochemical Properties. *Phys. Chem. Chem. Phys.* **2010**, *12*, 1649−1658.

(13) Noack, K.; Schulz, P. S.; Paape, N.; Kiefer, J.; Wasserscheid, P.; Leipertz, A. The Role of the C2 Position in Interionic Interactions of Imidazolium Based Ionic Liquids: A Vibrational and NMR Spectroscopic Study. *Phys. Chem. Chem. Phys.* **2010**, *12*, 14153−14161.

(14) Tsuzuki, S.; Tokuda, H.; Hayamizu, K.; Watanabe, M. Magnitude and Directionality of Interaction in Ion Pairs of Ionic Liquids: Relationship with Ionic Conductivity. *J. Phys. Chem. B* **2005**, *109*, 16474−16481.

(15) Lassègues, J.-C.; Grondin, J.; Cavagnat, D.; Johansson, P. New Interpretation of the CH Stretching Vibrations in Imidazolium-Based Ionic Liquids. *J. Phys. Chem. A* **2009**, *113*, 6419−6421.

(16) Grondin, J.; Lassègues, J. C.; Cavagnat, D.; Buffeteau, T.; Johansson, P.; Holomb, R. Revisited Vibrational Assignments of Imidazolium-Based Ionic Liquids. *J. Raman Spectrosc.* **2011**, *42*, 733−743.
(17) Wulf, A.; Fumino, K.; Ludwig, R. Spectroscopic Evidence for an Enhanced Anion−Cation Interaction from Hydrogen Bonding in Pure Imidazolium Ionic Liquids. *Angew. Chem., Int. Ed.* **2010**, *49*, 449−453.
(18) Fumino, K.; Wulf, A.; Ludwig, R. The Cation−Anion Interaction in Ionic Liquids Probed by Far-Infrared Spectroscopy. *Angew. Chem., Int. Ed.* **2008**, *47*, 3830−3834.
(19) Kempter, V.; Kirchner, B. The Role of Hydrogen Atoms in Interactions Involving Imidazolium-Based Ionic Liquids. *J. Mol. Struct.* **2010**, *972*, 22−34.
(20) Gao, Y.; Zhang, L.; Wang, Y.; Li, H. Probing Electron Density of H-Bonding between Cation−Anion of Imidazolium-Based Ionic Liquids with Different Anions by Vibrational Spectroscopy. *J. Phys. Chem. B* **2010**, *114*, 2828−2833.
(21) Akai, N.; Kawai, A.; Shibuya, K. First Observation of the Matrix-Isolated FTIR Spectrum of Vaporized Ionic Liquid: An Example of EmimTFSI, 1-Ethyl-3-methylimidazolium Bis-(trifluoromethanesulfonyl)imide. *Chem. Lett.* **2008**, *37*, 256−257.
(22) Akai, N.; Kawai, A.; Shibuya, K. Ion-Pair Structure of Vaporized Ionic Liquid Studied by Matrix-Isolation FTIR Spectroscopy with DFT Calculations: A Case of 1-Ethyl-3-methylimidazolium Trifluoromethanesulfonate. *J. Phys. Chem. A* **2010**, *114*, 12662−12666.
(23) Akai, N.; Parazs, D.; Kawai, A.; Shibuya, K. Cryogenic Neon Matrix-Isolation FTIR Spectroscopy of Evaporated Ionic Liquids: Geometrical Structure of Cation− Anion 1: 1 Pair in the Gas Phase. *J. Phys. Chem. B* **2009**, *113*, 4756−4762.
(24) Dong, K.; Zhao, L.; Wang, Q.; Song, Y.; Zhang, S. Are Ionic Liquids Pairwise in Gas Phase? A Cluster Approach and in situ IR Study. *Phys. Chem. Chem. Phys.* **2013**, *15*, 6034−6040.
(25) Earle, M. J.; Esperanca, J. M. S. S.; Gilea, M. A.; Canongia Lopes, J. N.; Rebelo, L. P. N.; Magee, J. W.; Seddon, K. R.; Widegren, J. A. The Distillation and Volatility of Ionic Liquids. *Nature* **2006**, *439*, 831−834.
(26) Chambreau, S. D.; Vaghjiani, G. L.; Koh, C. J.; Golan, A.; Leone, S. R. Ultraviolet Photoionization Efficiency of the Vaporized Ionic Liquid 1-Butyl-3-methylimidazolium Tricyanomethanide: Direct Detection of the Intact Ion Pair. *J. Phys. Chem. Lett.* **2012**, *3*, 2910−2914.
(27) Chambreau, S. D.; Boatz, J. A.; Vaghjiani, G. L.; Friedman, J. F.; Eyet, N.; Viggiano, A. A. Reactions of Ions with Ionic Liquid Vapors by Selected-Ion Flow Tube Mass Spectrometry. *J. Phys. Chem. Lett.* **2011**, *2*, 874−879.
(28) Koh, C. J.; Leone, S. R. Simultaneous Ion-Pair Photodissociation and Dissociative Ionization of an Ionic Liquid: Velocity Map Imaging of Vacuum-Ultraviolet-Excited 1-Ethyl-3-methylimidazolium Bis-(trifluoromethylsulfonyl)imide. *Mol. Phys.* **2012**, *110*, 1705−1712.
(29) Koh, C. J.; Liu, C.-L.; Harmon, C. W.; Strasser, D.; Golan, A.; Kostko, O.; Chambreau, S. D.; Vaghjiani, G. L.; Leone, S. R. Soft Ionization of Thermally Evaporated Hypergolic Ionic Liquid Aerosols. *J. Phys. Chem. A* **2011**, *115*, 4630−4635.
(30) Strasser, D.; Goulay, F.; Belau, L.; Kostko, O.; Koh, C.; Chambreau, S. D.; Vaghjiani, G. L.; Ahmed, M.; Leone, S. R. Tunable Wavelength Soft Photoionization of Ionic Liquid Vapors. *J. Phys. Chem. A* **2010**, *114*, 879−883.
(31) Ogura, T.; Akai, N.; Kawai, A.; Shibuya, K. Gas Phase Electronic Absorption Spectroscopy of Room Temperature Ionic Liquids: N-Ethyl-3-methylpyridinium or 1-Butyl-3-methylimidazolium Cation with Bis(trifluoromethylsulfonyl)amido Anion. *Chem. Phys. Lett.* **2013**, *555*, 110−114.
(32) Hunt, P. A.; Gould, I. R.; Kirchner, B. The Structure of Imidazolium-Based Ionic Liquids: Insights from Ion-Pair Interactions. *Aust. J. Chem.* **2007**, *60*, 9−14.
(33) Obi, E. I.; Leavitt, C. M.; Raston, P. L.; Moradi, C. P.; Flynn, S. D.; Vaghjiani, G. L.; Boatz, J. A.; Chambreau, S. D.; Douberly, G. E. Helium Nanodroplet Isolation and Infrared Spectrscopy of the Isolated Ion-Pair 1-Ethyl-3-methylimidazolium Bis-(trifluoromethylsulfonyl)imide. *J. Phys. Chem. A* **2013**, *117*, 9047−9056.
(34) Höfft, O.; Bahr, S.; Kempter, V. Investigations with Infrared Spectroscopy on Films of the Ionic Liquid [Emim]Tf2N. *Langmuir* **2008**, *24*, 11562−11566.
(35) Tsuzuki, S.; Tokuda, H.; Mikami, M. Theoretical Analysis of the Hydrogen Bond of Imidazolium C2-H with Anions. *Phys. Chem. Chem. Phys.* **2007**, *9*, 4780−4784.
(36) Luo, H. M.; Baker, G. A.; Dai, S. Isothermogravimetric Determination of the Enthalpies of Vaporization of 1-Alkyl-3-methylimidazolium Ionic Liquids. *J. Phys. Chem. B* **2008**, *112*, 10077−10081.
(37) Zaitsau, D. H.; Kabo, G. J.; Strechan, A. A.; Paulechka, Y. U.; Tschersich, A.; Verevkin, S. P.; Heintz, A. Experimental Vapor Pressures of 1-Alkyl-3-methylimidazolium Bis-(trifluoromethylsulfonyl)Imides and a Correlation Scheme for Estimation of Vaporization Enthalpies of Ionic Liquids. *J. Phys. Chem. A* **2006**, *110*, 7303−7306.
(38) Lasségues, J.-C.; Grondin, J.; Cavagnat, D.; Johansson, P. Reply to the "Comment on 'New Interpretation of the CH Stretching Vibrations in Imidazolium-Based Ionic Liquids'". *J. Phys. Chem. A* **2009**, *114*, 687−688.
(39) Wulf, A.; Fumino, K.; Ludwig, R. Comment on "New Interpretation of the CH Stretching Vibrations in Imidazolium-Based Ionic Liquids. *J. Phys. Chem. A* **2009**, *114*, 685−686.
(40) Zwier, T. S. Laser Spectroscopy of Jet-Cooled Biomolecules and Their Water-Containing Clusters: Water Bridges and Molecular Conformation. *J. Phys. Chem. A* **2001**, *105*, 8827−8839.
(41) Zwier, T. S. Laser Probes of Conformational Isomerization in Flexible Molecules and Complexes. *J. Phys. Chem. A* **2006**, *110*, 4133−4150.
(42) Dian, B. C.; Clarkson, J. R.; Zwier, T. S. Direct Measurement of Energy Thresholds to Conformational Isomerization in Tryptamine. *Science* **2004**, *303*, 1169.
(43) Wang, C.; Luo, H.; Li, H.; Dai, S. Direct UV-Spectroscopic Measurement of Selected Ionic-Liquid Vapors. *Phys. Chem. Chem. Phys.* **2010**, *12*, 7246−7250.
(44) Devine, A. L.; Cronin, B.; Nix, M. G.; Ashfold, M. N. High Resolution Photofragment Translational Spectroscopy Studies of the Near Ultraviolet Photolysis of Imidazole. *J. Chem. Phys.* **2006**, *125*, 184302.
(45) Barbatti, M.; Lischka, H.; Salzmann, S.; Marian, C. M. UV Excitation and Radiationless Deactivation of Imidazole. *J. Chem. Phys.* **2009**, *130*, 034305.
(46) Frisch, M. J.; Trucks, G. W.; Schlegel, H. B.; Scuseria, G. E.; Robb, M. A.; Cheeseman, J. R.; Scalmani, G.; Barone, V.; Mennucci, B.; Petersson, G. A.; et al. *Gaussian 09*, Revision D.01; Gaussian, Inc: Wallingford, CT, 2009.
(47) Zhao, Y.; Truhlar, D. The M06 Suite of Density Functionals for Main Group Thermochemistry, Thermochemical Kinetics, Noncovalent Interactions, Excited States, and Transition Elements: Two New Functionals and Systematic Testing of Four M06-Class Functionals and 12 Other Functionals. *Theor. Chem. Acc.* **2008**, *120*, 215−241.
(48) The augmented correlation consistent polarized valence triple-ζ basis (aug-cc-pVTZ) was used for all atoms except sulfur, for which the aug-cc-pV(T+d)Z basis set was utilized.
(49) Pople, J. A.; Binkley, J. S.; Seeger, R. Theoretical Models Incorporating Electron Correlation. *Int. J. Quantum Chem., Symp.* **1976**, *S10*, 1−19.
(50) Kendall, R. A.; Dunning, T. H., Jr.; Harrison, R. J. Electron Affinities of the First-Row Atoms Revisited. Systematic Basis Sets and Wave Functions. *J. Chem. Phys.* **1992**, *96*, 6796.
(51) Dunning, T. H., Jr.; Peterson, K. A.; Wilson, A. K. Gaussian Basis Sets for Use in Correlated Molecular Calculations. X. The Atoms Aluminum through Argon Revisited. *J. Chem. Phys.* **2001**, *114*, 9244.
(52) Frisch, M. J.; Head-Gordon, M.; Pople, J. A. A Direct MP2 Gradient Method. *Chem. Phys. Lett.* **1990**, *166*, 275−280.

(53) Dunning, T. H., Jr. Gaussian Basis Sets for Use in Correlated Molecular Calculations. I. The Atoms Boron through Neon and Hydrogen. *J. Chem. Phys.* **1989**, *90*, 1007−1023.
(54) Aikens, C. M.; Webb, S. P.; Bell, R. L.; Fletcher, G. D.; Schmidt, M. W.; Gordon, M. S. A Derivation of the Frozen-Orbital Unrestricted Open-Shell and Restricted Closed-Shell Second-Order Perturbation Theory Analytic Gradient Expressions. *Theor. Chem. Acc.* **2003**, *110*, 233−253.